

Observations of 44 extragalactic radio sources with the VLBA at 92cm:

A List of Potential Calibrators and Targets for LOFAR and RadioAstron

H. Rampadarath^{*1,3}, M.A. Garrett^{**2,3,4}, and A. Polatidis^{***1,2}

¹ Joint Institute for VLBI in Europe (JIVE), Postbus 2, 7990 AA Dwingeloo, The Netherlands

² Netherlands Institute for Radio Astronomy (ASTRON), Postbus 2, 7990 AA Dwingeloo, The Netherlands

³ Sterrewacht Leiden, Leiden University, Oort Building, Neils Borweg 2, 2333 CA, Leiden, The Netherlands

⁴ Centre for Supercomputing, Swinburne University of Technology, Mail number H39, P.O. Box 218, Hawthorn, Victoria 3122, Australia

Received February 2, 2009; Accepted March 14, 2009

ABSTRACT

Aims. We have analysed VLBA 92cm archive data of 44 extragalactic sources in order to identify early targets and potential calibrator sources for the LOFAR radio telescope and the RadioAstron space VLBI mission. Some of these sources will also be suitable as “in-beam” calibrators, permitting deep, wide-field studies of other faint sources in the same field of view.

Methods. All publicly available VLBA 92cm data observed between 1 January 2003 to December 31 2006 have been analysed via an automatic pipeline, implemented within AIPS. The vast majority of the data are unpublished.

Results. The sample consists of 44 sources, 34 of which have been detected on at least one VLBA baseline. 30 sources have sufficient data to be successfully imaged. Most of the sources are compact, with a few showing extended structures. Of the 30 sources imaged, 13 are detected on the longest VLBA baselines ($\sim 9 M\lambda$), while all were detected on baselines greater than $2 M\lambda$ (the maximum baseline of LOFAR including the current international baselines).

Key words. Radiation mechanisms: general – Radio continuum: general – Techniques: interferometric

1. Introduction

Low-frequency observations of the radio sky are set to be transformed by a new generation of radio telescopes. In particular, instruments such as LOFAR (the Low Frequency Array) will permit large areas of the sky to be surveyed at very low-frequencies (30-230 MHz) with unprecedented sensitivity, and with arcsecond and sub-arcsecond resolution. The base LOFAR configuration foresees at least 36 stations being distributed across the Netherlands with at least 9 additional international stations located in Germany (5), Sweden (1), France (1), the UK (1) and Italy (1). Further stations are planned in other European countries, including Poland, Austria, Ireland and the Ukraine (Garrett et al. 2009). Initial science observations with LOFAR are expected to begin in 2009.

The extension of LOFAR to baseline lengths of a few thousand kilometres presents several new challenges. With a resolution of up to ~ 0.2 arcseconds, the sky density of suitable calibrator sources may be a significant issue especially at the lowest frequencies. In particular, very little is known about the morphology of radio sources at these low frequencies and high resolutions. A very similar situation exists with the space

VLBI mission RadioAstron, due to be launched in October 2009 (Zakharov 2007). With a maximum baseline length of 350,000 km, RadioAstron will have a fringe spacing of 0.540 milliarcseconds at 327 MHz (see the RadioAstron booklet for more details¹).

Altschuler et al. (1995) presented the results of a global Mark II VLBI 92 cm snapshot survey. Their sample contained 16 sources, of which there were 3 radio galaxies: 0116+319 (4C31.04), 1117+146 (4C14.41), 2050+364 (DA529); 4 BL Lac objects: 0235+164, 0723-008, 0735+178, 0851+202 (OJ287); and 9 quasars: 0333+321 (NRAO140), 1055+018 (4C01.28), 1422+202, 1611+343 (DA406), 1633+382 (4C38.41), 1901+319 (3C395), 2145+067 (4C06.69), 2230+114 (CTA102), 2251+158 (3C454.3). All of which were resolved on baselines longer than 2-6 $M\lambda$. Only 2 of the sources observed by altetal95 (3C395 and 3C454.3) are part of the sample presented in this paper.

Chuprikov et al. (1999) have presented a list of 61 sources, observed in two separate experiments, at 327 MHz with a global Mark II VLBI array. Of the 61 sources observed, 25 were recommended for further detailed observations and images were made of 2 of these sources. 3 of the sources we present in this paper

* e-mail: rampadarath@jive.nl

** e-mail: garrett@astron.nl

*** e-mail: polatidis@astron.nl

¹ <http://www.asc.rssi.ru/radioastron>

(3C273, 3C345 and BL Lac), are also included in Chuprikov's sample.

Lenc et al. (2008) have conducted a deep wide field VLBI survey of the sky at 92cm with a global VLBI array using two in-beam calibrators. Of the 272 potentially detectable targets, about 20 sources show compact, milliarcsecond scale structures. These results are encouraging, and suggest that deep, wide-field studies of relatively faint radio sources (using suitable in-beam calibrators) should be a productive way of characterising the low-frequency radio sky at the highest resolution.

All these developments, emphasise the need to establish a suitable list of compact radio sources that may be good calibrators or reasonable commissioning targets for LOFAR and the RadioAstron mission. In this paper, we present the results of an automatic analysis of 327 MHz data publicly available via the NRAO Very Long Baseline Array (VLBA), observed during the period 1 January 2003 - 31 December 2006². In Section 2 we discuss the automatic pipeline procedure, and in section 3 we present the main results of our analysis, including images of the individual sources. Notes and brief descriptions of some interesting sources are presented as a separate appendix. Final conclusions are also drawn in section 3.

2. Data analysis

All publicly available VLBA 327 MHz data, observed during the period 1 January 2003 - 31 December 2006 were downloaded from the archive and processed by an automatic pipeline implemented in NRAO's AIPS. 23 individual projects were processed (not including many multi-epoch sub-projects), comprising a total of 44 unique radio sources. Table 1 lists the various projects, and the sources observed. 8 of the 23 projects included multiple-pass correlation (see Table 1) to target multiple sources in the same field of view. Table 2 gives details of the individual sources. The sources in the sample are located fairly randomly on the northern sky, with a range of declinations from $\delta = -33$ degrees to $\delta = +77$ degrees. The pipeline was designed to amplitude calibrate the data and fringe fit each source individually, using a solution interval of 3 minutes in all cases. The data were averaged in time and frequency, after applying the initial calibration. The pipeline also produced preliminary images of each amplitude calibrated and fringe-fitted (detected) source. For those sources detected, manual editing and imaging was conducted using the AIPS tasks CALIB and IMAGR.

Of the 44 sources, 34 were detected on all or some subset of VLBA baselines (table 3) and 10 sources were not detected, on any VLBA baseline: J0440-4333, J0959+6932 (M82), J0955+6940; J1159+0112, J1230-1139, J2007+4029, J2322+0812, J2236+2828, J2334+0736 and J2344+3433. 30 were successfully imaged and 4 sources were either severely resolved or did not have enough data (or UV-coverage) to be successfully imaged. One special case is Cygnus-A. This was barely detected (9σ) only on the shortest VLBA baseline, and only by introducing an offset point model. For complex sources like Cygnus-A, a more complex model within FRING might result in more detections.

² The National Radio Astronomy Observatory is a facility of the National Science Foundation operated under cooperative agreement by Associated Universities, Inc

3. Results and discussion

Table 3 lists the sources that were detected. Note that most sources were observed by more than 1 project (see table 1). In these cases, the "best" observation was selected, based on quality and quantity of the data. Figures 1-5 show the contour plots of the sources³. Given that the longest LOFAR baseline at 240 MHz, corresponds to $2M\lambda$, all sources that are detected on all VLBA baselines are also likely to be detected by LOFAR. All of the 30 sources imaged, are compact enough to be detected on baselines greater than $2M\lambda$, and many show extended structures and are resolved even beyond this baseline length (e.g. see 3C84, Figure 1). However, for LOFAR, many of these sources will remain unresolved (see the amplitude vs UV-distance plots presented in Figures 1-8). Many of the sources imaged in our programme should therefore make excellent LOFAR primary phase/bandpass calibrators, especially on the longest LOFAR baselines. Table 4 lists the best candidate calibrators.

Of the 30 imaged sources, only 13 sources have been detected on the very longest VLBA baselines (9-9.5 $M\lambda$). These 13 sources may prove to be interesting targets for RadioAstron. In particular, sources such as 3C84, 1148-001, J2330+11,1510-089,0537-286 and 3C345 may be employed as "in-beam" calibrators for deep wide-field 327 MHz ground based VLBI observations. These sources are strong enough to be well detected by ground based VLBI arrays, but not so bright as to significantly raise the system noise of the antennas or introduce potential dynamic range limitations in the image plane.

It is interesting to note how the morphology of some of the sources in our sample change with baseline length. A good example is Cygnus-A. The first observations taken with the LOFAR test station at Exloo (1 km baseline) show that Cygnus-A is one of the brightest objects in the sky. However, the VLBA observations at 327 MHz do not detect Cygnus-A on all but the shortest (240 km) baseline (using an offset point source model centred on one of the lobes, see the Appendix for further discussion). We conclude that Cygnus-A will also be heavily resolved for LOFAR on the longest international baselines, at least at the highest observing frequencies. In particular, there is no guarantee that sources that make good calibrators for the LOFAR core, will also be appropriate for longer baseline lengths. Other bright sources will no-doubt show similar properties, although we also note that some of these bright sources (e.g. 3C274) remain bright and compact on milliarcsecond scales.

More systematic surveys by the VLBA at 327 MHz would be useful to further extend the list of potential calibrators and targets for both LOFAR and RadioAstron.

APPENDIX: Individual source comments

In this Appendix the properties of some of the more interesting sources in our sample are discussed.

J0405+3803

The data presented in this paper for J0405+3803, have previously been observed and published by Rodriguez et al. (2006). The images of 0402+379 produced in this article, compare well with those of Rodriguez et al. (2006), and are consistent with lower resolution VLA images taken at 1.4 GHz (Xu et al. 1995).

³ The corresponding plots of flux density against UV-distance and U vs V plots, will be available on the electronic version

J0433+0521 (3C120)

The VLBA images at 327 MHz presented here are consistent with the images at 2.3 GHz taken by Fey & Charlot (2000), also using the VLBA. The results at 2.3 GHz presents the core and jet of 3C120 with 3 jet components, all located within approximately 100 mas of the core. The results presented here show an extended jet that spans sin 300 mas.

J0542+4951 (3C147)

3C147 is very resolved at 327 MHz and shows an elongated structure that spans ~ 400 milliarcseconds, largely consistent with that observed by EVN-MERLIN at 1.6 GHz (Davis et al. 1996). The image is also in good agreement with higher resolution VLBA observations made at 8.5 GHz and 2.3 GHz (Fey & Charlot 2000). We do not detect the emission seen by MERLIN to the North-East of the peak emission, that (Davis et al. 1996) interpret as evidence of outflow from a counter jet. There is also an extended structure to the South-East of the peak of the emission, which is also observed at 1.6 GHz with EVN-MERLIN and, 2.3/8.5 GHz (VLBA).

J1230+1223 (M87, 3C274)

The observations with the VLBA at 327 MHz show that the well-known jet extends up to ~ 500 mas (0.5 arcsecs) from the core. The superluminal component observed by the Hubble Space Telescope known as HST 1, (Biretta et al. 1999) is clearly detected, located approximately 0.8 arcsecs from the core. This has also recently been detected by the VLBA at 15 GHz (Chang et al. 2008). At 15 GHz HST-1 appears to be variable. When detected it has a flux density in the range of 14-22 mJy. At 327 MHz, we measure an integrated flux density of 317 mJy, implying a spectral index of $\alpha_{0.327}^{15} \sim -0.697$. The size of the component at 327 MHz is 48×21 milliarcseconds in PA ~ 144 degrees.

J1331+3030 (3C286)

Our images of 3C286 are consistent with other VLBA images at higher frequencies e.g. Fey & Charlot (2000). The 327 MHz observations are clearly extended in the same direction as that seen in the MERLIN images at 18 cm (Akujor et al. 1994). We do not see the counter jet report by (Akujor et al. 1994).

J1512-0905

The image presented here at 327 MHz shows a jet component to the North-East of the core, which ends in a hot-spot. At higher frequencies (2.3, 8.6 and 15 GHz), the hot-spot is not visible by the VLBA, but there is evidence for a jet component along the direction of the hot-spot (Fey & Charlot 1997; Lister & Homan 2005).

J1746+6226 (4C +62.29)

At 327 MHz, we observe an extended core component with a morphology that is consistent with higher frequency VLBA observations at 2.3 GHz and 8.6 GHz Fey & Charlot (2000). However, our images also reveal a counter jet with a hot-spot located approximately 0.2 arcseconds to the North-East of the extended core. The PA of this counter jet feature is diametrically

opposite to the higher frequency jet that is seen on the other side of the core.

J1829+4844 (3C380)

The radio source J1829+4844 is identified with the very powerful steep spectrum radio source, 3C380. Observations at decimetre and centimetre wavelengths have identified this object as an FR II source that is elongated along the line-of-sight (Wilkinson et al. 1991; Megn et al. 2006). This source has a very extended structure, with a number of compact components that corresponds to the core coincident with the optical quasar with a short (15 mas) jet, a hot-spot in the nearer lobe 0.7 arcseconds from the core, and another slightly larger hot-spot 0.4 arcseconds from the first (Megn et al. 2006). The lobes are located to the North-West of the core. Only the core and the hot-spot at 0.7 arcseconds from the core are visible in the VLBA observations at 327 MHz.

J1902+3159 (3C395)

3C395 is identified with a 17th magnitude quasar (Gelderman & Whittle 1994), and has a complex radio structure on a wide range of angular scales. At 8.3 GHz with the VLBA its core-jet radio structure consists of two components (core and a hot-spot) separated by approximately 15 mas, with the hot-spot located South-West of the core (Lara et al. 1997). VLBI images at 326 MHz, taken by Altschuler et al. (1995) show a compact and unresolved core, and an extended regio of emission separated by approximately 65 mas South-West of the core. Our results agree well with these low resolution images. There is also a fainter, extended component observed in our image at P.A. 111.7° . This was not observed by Altschuler et al. (1995).

J1959+4044 (Cygnus-A)

Despite being one of the brightest sources in the sky, Cygnus A was not detected by the VLBA at 327 MHz, except on the shortest baselines after including an offset point source model for the FRING task - offset in the direction of the South-Eastern lobe. Since it is located at low galactic latitude ($b = 5$ degrees), the core of Cygnus-A may be scatter broadened due to interstellar scattering in our own galaxy (Carilli et al. 1991). With a measured size of 1.6 mas at 5 GHz, we would expect the core size to be ~ 400 mas at 327 MHz. The core of Cygnus-A is therefore likely to be resolved by our observations. The same may also be true of hot-spots in the two lobe structures.

Acknowledgements. This research was supported by the EU Framework 6 Marie Curie Early Stage Training programme under contract number MEST-CT-2005-19669 "ESTRELA".

References

- Akujor, C. E., Luedke, E., Browne, I. W. A., et al. 1994, A&AS, 105, 247
 Altschuler, D. R., Gurvits, L. I., Alef, W., et al. 1995, A&AS, 114, 197
 Biretta, J. A., Sparks, W. B., & Macchetto, F. 1999, ApJ, 520, 621
 Carilli, C. L., Bartel, N., & Linfield, R. P. 1991, AJ, 102, 1691
 Chang, C. S., Ros, E., Kovalev, Y. Y., & Lister, M. L. 2008, astro-ph/0812.0126
 Chuprikov, A. A., Girin, I. A., Likhachev, S. F., et al. 1999, New Astronomy Review, 43, 747
 Davis, R. J., Diamond, P. J., & Goss, W. M. 1996, MNRAS, 283, 1105
 Fey, A. L. & Charlot, P. 1997, ApJS, 111, 95
 Fey, A. L. & Charlot, P. 2000, ApJS, 128, 17
 Garrett, M. A., Rampadarath, H., Lenc, E., & Wucknitz, O. 2009, astro-ph/0902.2534v2
 Gelderman, R. & Whittle, M. 1994, ApJS, 91, 491

- Lara, L., Muxlow, T. W. B., Alberdi, A., et al. 1997, *A&A*, 319, 405
- Lenc, E., Garrett, M. A., Wucknitz, O., Anderson, J. M., & Tingay, S. J. 2008, *ApJ*, 673, 78
- Lister, M. L. & Homan, D. C. 2005, *AJ*, 130, 1389
- Megn, A. V., Rashkovskii, S. L., Shepelev, V. A., et al. 2006, *Astronomy Reports*, 50, 692
- Rodriguez, C., Taylor, G. B., Zavala, R. T., et al. 2006, *ApJ*, 646, 49
- Wilkinson, P. N., Akujor, C. E., Cornwell, T. J., & Saikia, D. J. 1991, *MNRAS*, 248, 86
- Xu, W., Readhead, A. C. S., Pearson, T. J., Polatidis, A. G., & Wilkinson, P. N. 1995, *ApJS*, 99, 297
- Zakharov, A. F. 2007, *Serbian Astronomical Journal*, 174, 1

Table 1. 327 MHz VLBA archived projects from 2003 to 2006

Project	Date of Observation	Common Source name
BM201B	16/07/03	3C454.3, J2327+0940, J2334+0736, J2336+2828
BM193 PASS1	30/08/03	NGC 7674, J2330+1100, 3C454.3
BM193 PASS2	30/08/03	J2322+081, J2330+11, 3C454.3
BC138A PASS1	09/08/03	J1331+3030, 3C336, J1816+3457
BC138A PASS2	09/08/03	J1331+3030, J1619+2247, J1816+3457
BEO32A PASS1	09/11/03	3C286, 3C395, 3C418, 3C454.3, BLLAC, Cygnus-A, J1821+3945, J1829+4844, J1924+3329, J2007+4029
BEO32A PASS2	09/11/03	3C286, 3C395, 3C418, 3C454.3, BLLAC, J2007+4029, J1821+3945, J1829+4844, J1924+3329, J2007+4029
BWO67Q	31/12/03	3C120, 3C286, 3C147, J0423-0120
BC138C	30/01/04	3C273, 3C275.1, J1331+3030
BH116	11/03/04	3C286;J1512-0905
BJ046R	23/04/04	J1150-0024, 3C147, 3C274
BB197	08/07/04	3C454.3, J2022+6136, J1829+4844
BH126A	23/12/04	3C147, J1150-002
BC150	11/02/05	J1746+6226, 3C286, 3C345
BT070B	13/06/05	J0405+3803, 3C111, 3C84
BFO87 PASS1	03/12/05	J2005+7752, J0955+6940
BFO87 PASS2	03/12/05	M82, J2005+7752
BH135D	06/02/06	J0955+6940, J1150-002, 3C147, 3C274
BK131C	08/06/06	J1230-1139, J1333+1649, 3C286, 3C345, J0539-283
BK131A	09/06/06	J0440-4333, J0204+3649, J0319+4130, J2344+3433, J0405+3803, 3C454.3
BK131B	18/06/06	J0440-4333, J1159+0112, 3C286, J0539-2839, J2344+3433, 3C454.3
BH135G	03/07/06	J1150-0024, 3C147, 3C274

Table 2. General properties of the 44 radio sources detected by VLBA at 92cm from 2003-2006. *Obtained from The NASA Extragalactic Database*

IAU J2000 Source Name	Other Aliases	Type	Redshift	R. A. (J2000)	Decl. (J2000)
J0204+3649	0201+365	Q	2.912000	02h04m55.596s	+36d49m17.996s
J0319+4130	3C84	G	0.017559	03h19m48.160s	+41d30m42.103s
J0405+3803	4C+37.11	G	0.055000	04h05m49.262s	+38d03m32.236s
J0407-3303	0405-331	Q	2.562000	04h07m33.914s	-33d03m46.359s
J0418+3801	3C111	G	0.048500	04h18m21.277s	+38d01m35.900s
J0423-0120	-	Q	0.914000	04h23m15.801s	-01d20m33.065s
J0433+0521	3C120	G	0.033100	04h33m11.096s	+05d21m15.619s
J0440-4333	0438-436	Q	2.863000	04h40m17.180s	-43d33m08.604s
J0542+4951	3C147	Q	0.545000	05h42m36.138s	+49d51m07.234s
J0539-2839	0537-286	Q	3.104000	05h39m54.281s	-28d39m55.948s
J0959+6932	M82	G	0.000677	09h59m10.639s	+69d32m17.724s
J0955+6940	-	-	-	09h59m55.694	+69d40m43.690s
J1150-0024	1148-001	Q	1.976200	11h50m43.871s	-00d23m54.205s
J1230+1223	3C274, M87	G	0.004360	12h30m49.423s	+12d23m28.044s
J1159+0112	1157+014	Q	1.999650	11h59m44.829s	+01d12m06.960s
J1229+0203	3C273	Q	0.158339	12h29m06.700s	+02d03m08.598s
J1230-1139	1228-113	Q	3.528000	12h30m55.556s	-11d39m09.796s
J1243+1622	3C275.1	Q	0.555100	12h43m57.657s	+16d22m53.440s
J1331+3030	3C286	G	0.586000	13h31m08.288s	+30d30m32.959s
J1333+1649	1331+170	Q	2.084000	13h33m35.783s	+16d49m04.015s
J1512-0905	1510-089	Q	0.360000	15h12m50.533s	-09d05m59.829s
J1619+2247	-	Q	1.987000	16h19m14.825s	+22d47m47.85s
J1624+2345	3C336	Q	0.927398	16h24m39.088s	+23d45m12.240s
J1642+3948	3C345	Q	0.592800	16h42m58.810s	+39d48m36.994s
J1746+6226	4C+62.29	Q	3.889000	17h46m14.034s	+62d26m54.738s
J1816+3457	-	G	0.244800	18h16m23.901s	+34d57m45.748s
J1821+3945	-	RS	-	18h21m59.701s	+39d45m59.657s
J1829+4844	3C380	Q	0.692000	18h29m31.739s	+48d44m46.971s
J1902+3159	3C395	Q	0.635000	19h02m55.939s	+31d59m41.702s
J1924+3329	4C+33.48	RS	-	19h24m17.476s	+33d29m29.484s
J1959+4044	Cygnus-A	Q	0.056075	19h59m28.357s	+40d44m02.097s
J2005+7752	2007+777	Q	0.342000	20h05m30.999s	+77d52m43.248s
J2007+4029	2005+403	Q	1.736000	20h07m44.945s	+40d29m48.604s
J2022+6136	-	G	0.227000	20h22m06.682s	+61d36m58.805s
J2038+5119	3C418	Q	1.686000	20h38m37.035s	+51d19m12.663s
J2202+4216	BL Lac	Q	0.068600	22h02m43.291s	+42d16m39.980s
J2253+1608	3C454.3	Q	0.859000	22h53m57.748s	+16d08m53.561s
J2322+0812	2320+079	Q	2.090000	23h22m36.089s	+08d12m01.593s
J2327+0846	NGC7674	G	0.028924	23h27m56.710s	+08d46m44.135s
J2327+0940	-	Q	1.843000	23h27m33.581s	+09d40m09.463s
J2330+1100	-	Q	1.489000	23h30m40.852s	+11d00m18.710s
J2334+0736	-	Q	0.401000	23h34m12.828s	+07d36m27.552s
J2336+2828	-	RS	-	23h36m22.471s	+28d28m57.413s
J2344+3433	2342+342	Q	3.053000	23h44m51.254s	+34d33m48.640s

Table 3. List of 34 detected sources. The images of most of these sources are shown in Figures 1-5.

Source	Detected Baseline (M λ)	Imaged (Y/N)	Peak Flux Density (Jy/beam)	Total Flux Density, S_{327} (Jy)
J0204+3649	8.0	Y	0.337	0.481
J0319+4130 (3C84)	9.0	Y	2.289	4.625
J0405+3803	4.0	Y	0.427	0.539
J0407-3303	9.5	Y	0.200	0.225
J0418+3801 (3C111)	6.0	Y	0.328	0.533
J0423-0120	9.5	Y	0.869	1.099
J0433+0521 (3C120)	9.5	Y	1.263	1.771
J0542+4951 (3C147)	8.0	Y	3.850	40.980
J0539-2839	9.5	Y	0.498	0.564
J1150-0024	9.5	Y	2.645	3.403
J1230+1223 (3C274)	9.5	Y	1.199	2.154
J1229+0203 (3C273)	9.5	Y	4.028	5.23
J1243+1622 (3C275.1)	2.0	Y	0.422	1.413
J1331+3030 (3C286)	9.5	Y	6.289	16.926
J1333+1649	6.0	Y	0.043	0.474
J1512-0905	9.5	Y	0.480	0.611
J1619+2247	2.5	N	-	-
J1624+2345 (3C336)	4.5	N	-	-
J1642+3948 (3C345)	9.5	Y	2.952	3.492
J1746+6226	6.5	Y	0.038	0.131
J1816+3457	6.0	Y	0.440	0.729
J1821+3945	5.0	Y	1.748	3.974
J1829+4844	8.0	Y	2.948	3.880
J1902+3159 (3C395)	5.0	Y	0.842	2.100
J1924+3329	2.0	Y	0.826	0.940
J1959+4044 (Cygnus-A)	0.3	N	-	-
J2005+7752	6.0	Y	0.508	0.602
J2022+6136	9.5	Y	0.635	0.990
J2038+5119 (3C418)	4.0	Y	1.234	3.320
J2202+4216 (BL Lac)	6.0	Y	0.938	1.798
J2253+1608 (3C454.3)	9.0	Y	5.300	8.659
J2327+0846 (N7674)	1.8	N	-	-
J2327+0940	7.0	Y	0.317	0.396
J2330+1100	9.0	Y	0.774	0.844

Table 4. Best primary candidate calibrators for LOFAR on baselines $\sim 2M\lambda$.

Source	Type	Redshift	R.A.	Dec.	S_{327} (Jy)
J0319+4130 (3C84)	Q	0.017559	03h19m48.160s	+41d30m42.103s	4.625
J0405+3803	G	0.055000	04h05m49.262s	+38d03m32.236s	0.539
J0418+3801 (3C111)	G	0.048500	04h18m21.277s	+38d01m35.900s	0.533
J0423-0120	Q	0.914000	04h23m15.801s	-01d20m33.065s	1.099
J0539-2839	Q	3.104000	05h39m54.281s	-28d39m55.948s	0.564
J1150-0024	Q	1.976200	11h50m43.871s	-00d23m54.205s	3.403
J1642+3948 (3C345)	Q	0.592800	16h42m58.810s	+39d48m36.994s	3.492
J1816+3457	G	0.244800	18h16m23.901s	+34d57m45.748s	0.729
J2005+7752	Q	0.342000	20h05m30.999s	+77d52m43.248s	0.602
J2022+6136	G	0.227000	20h22m06.682s	+61d36m58.805s	0.990
J2202+4216 (BL Lac)	Q	0.068600	22h02m43.291s	+42d16m39.980s	1.798
J2253+1608 (3C454.3)	Q	0.859000	22h53m57.748s	+16d08m53.561s	8.659
J2327+0940	Q	1.843000	23h27m33.581s	+09d40m09.463s	0.396
J2330+1100	Q	1.489000	23h30m40.852s	+11d00m18.710s	0.844

Fig. 1. Imaged sources at 327 MHz. The sources here in order are: J0204+3649, J0319+4130 (3C84), J0405+3803, J0407-3303, J0418+3801 (3C111), J0423-0120

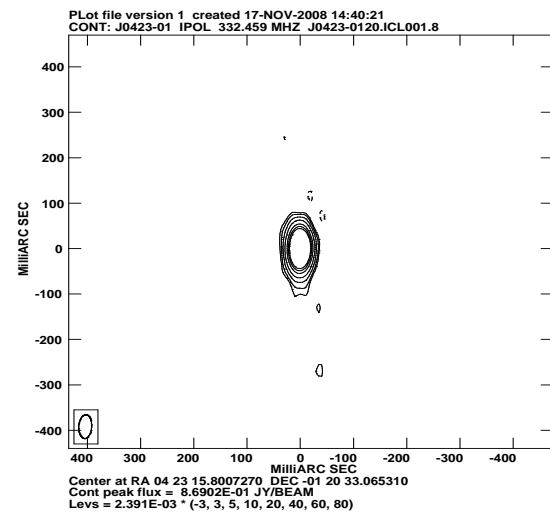
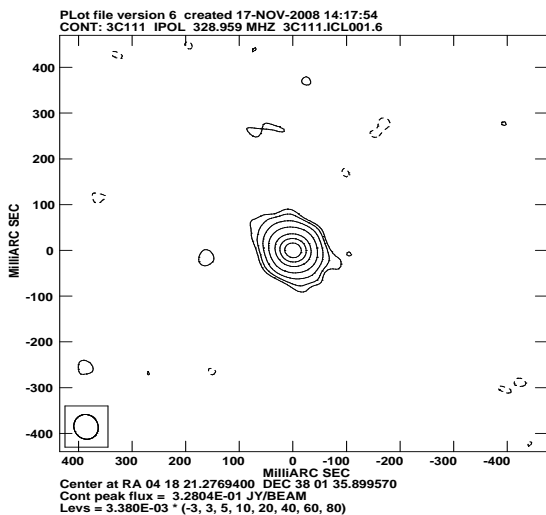
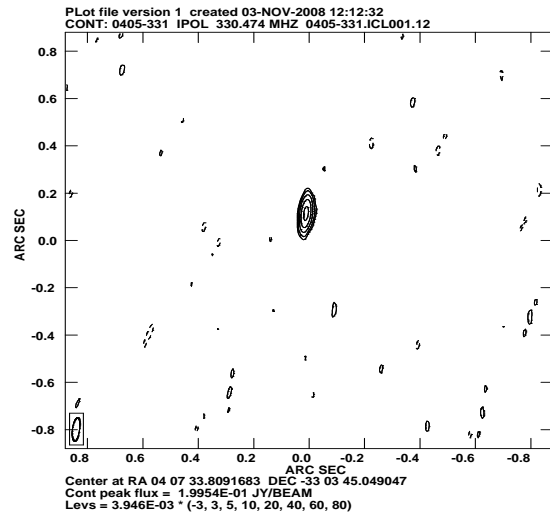
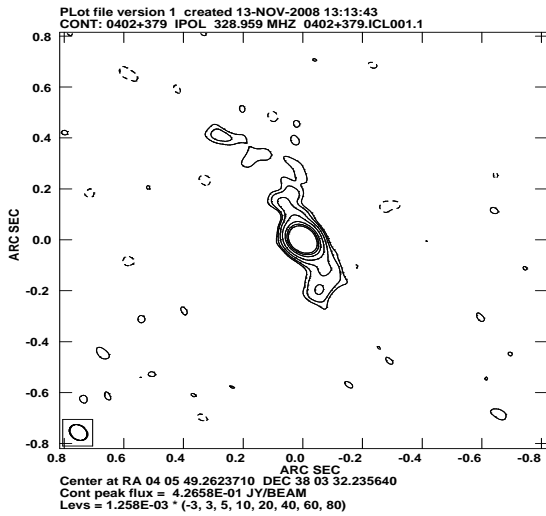
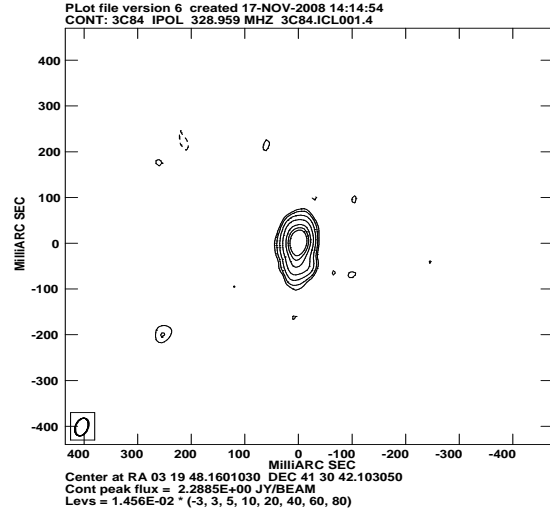
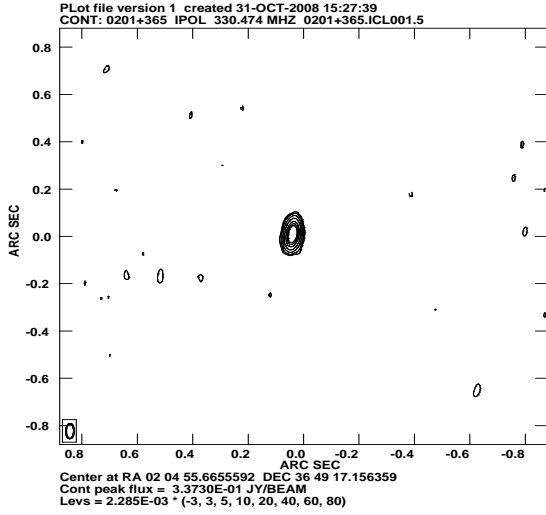


Fig. 2. Imaged sources at 327 MHz. The sources here in order are: J0433+0521 (3C120), J0542+4951 (3C147), J0539-2839, J1150-0024, J1230+1223 (3C274), J1229+0203 (3C273)

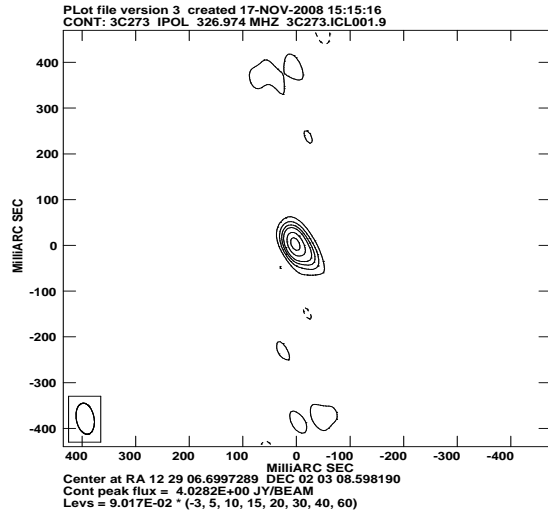
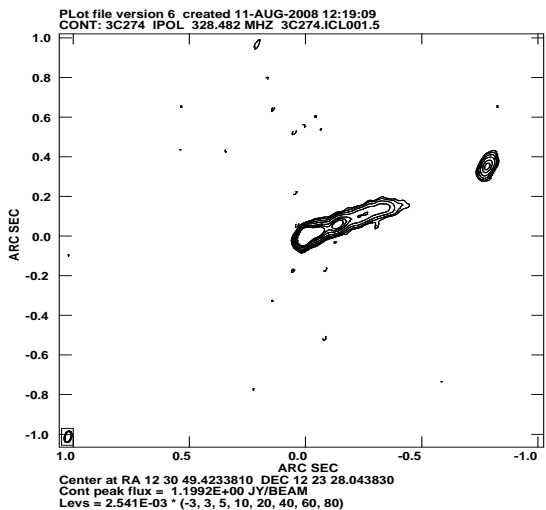
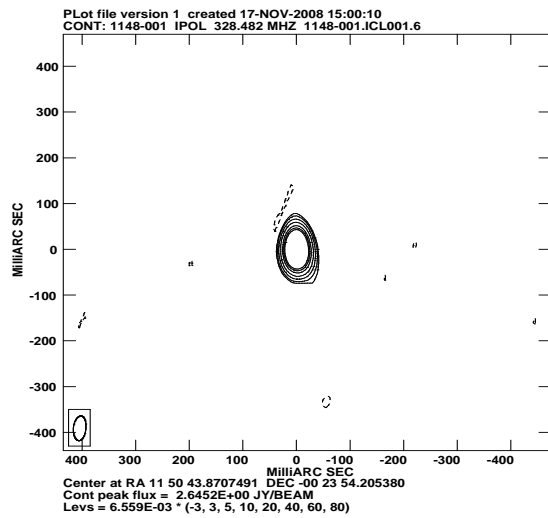
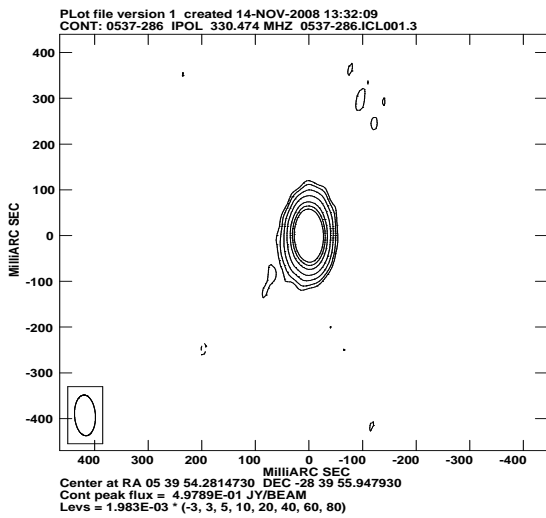
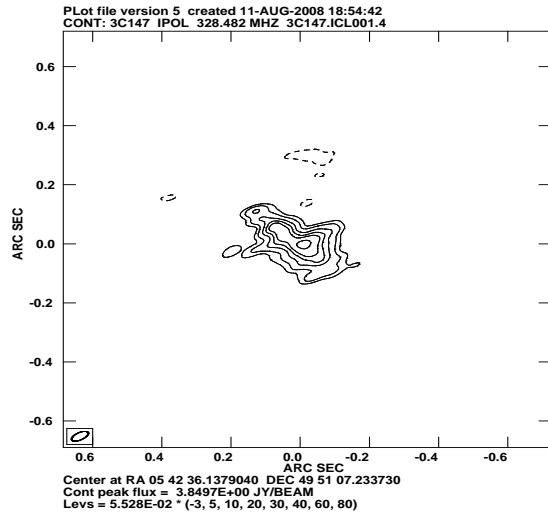
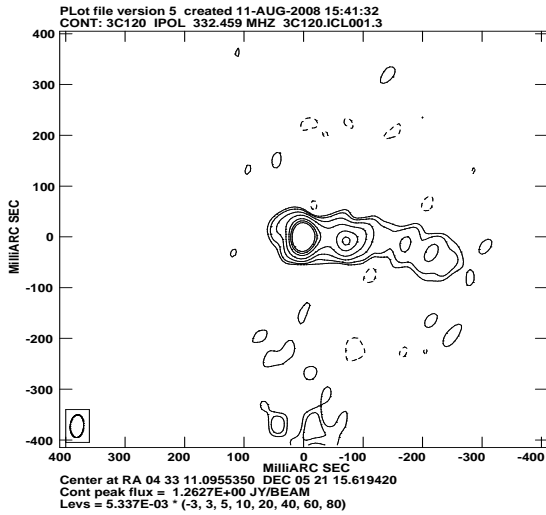


Fig. 3. Imaged sources at 327 MHz. The sources here in order are: J1243+1622 (3C275.1), J1331+3030 (3C286), J1333+1649, J1512-0905, J1642+3948 (3C345), J1746+6226

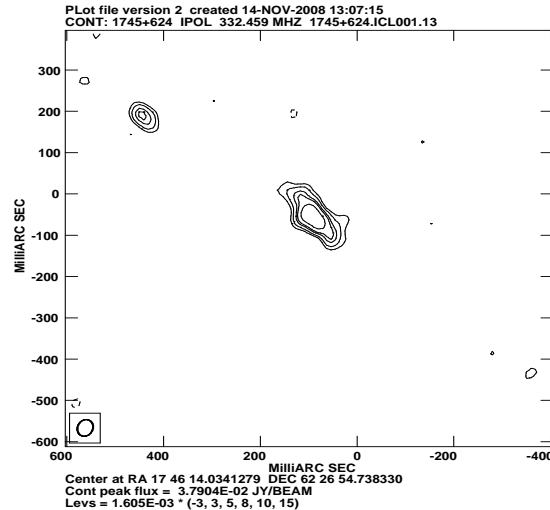
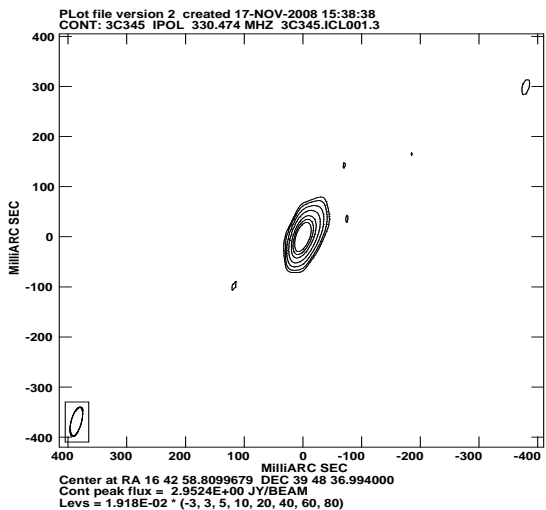
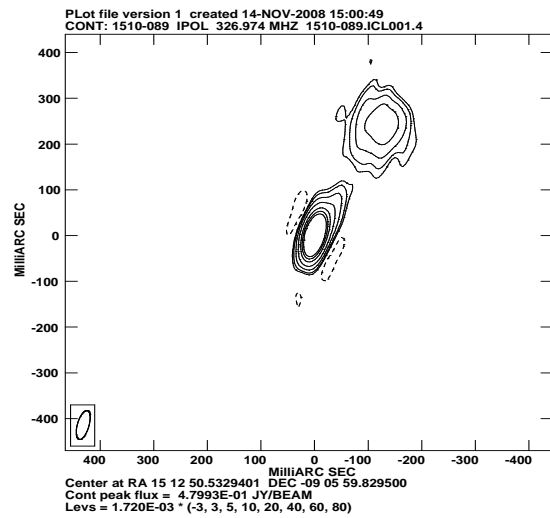
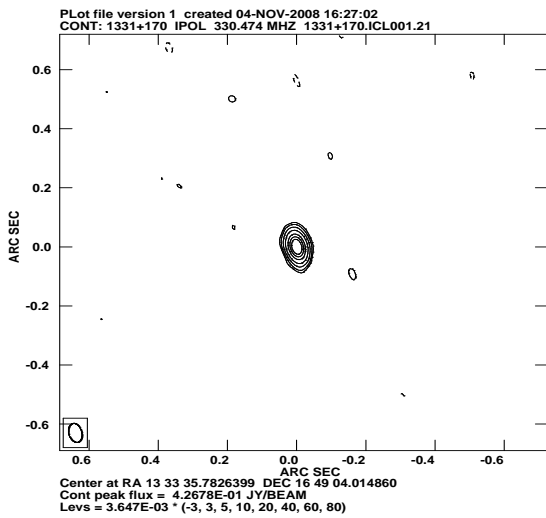
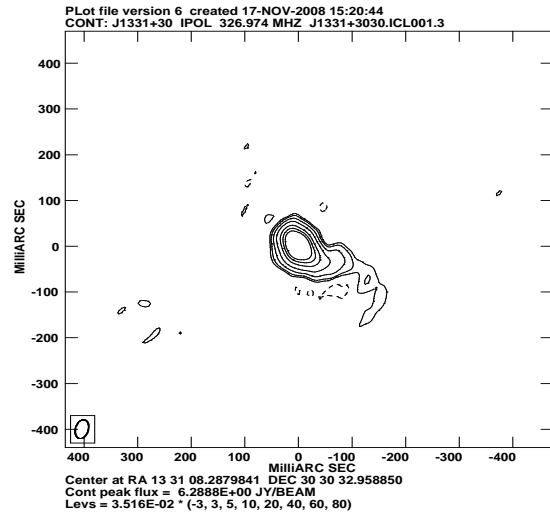
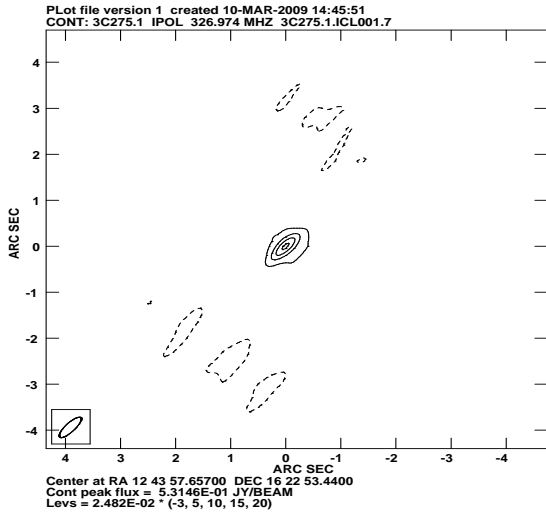


Fig. 4. Imaged sources at 327 MHz. The sources here in order are: J1816+3457, J1821+3945, J1829+4844, J1902+3159 (3C395), J1924+3329, J2005+7752

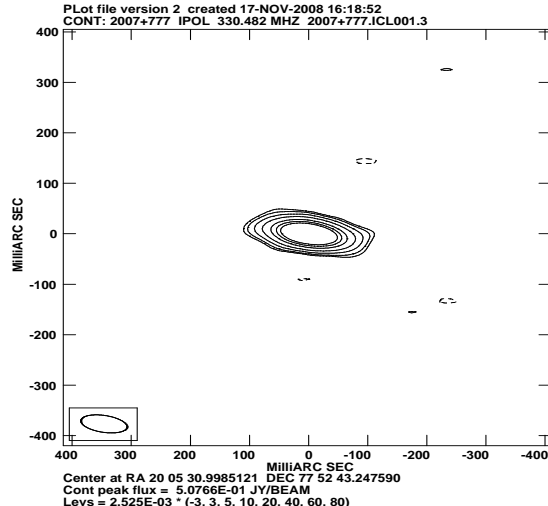
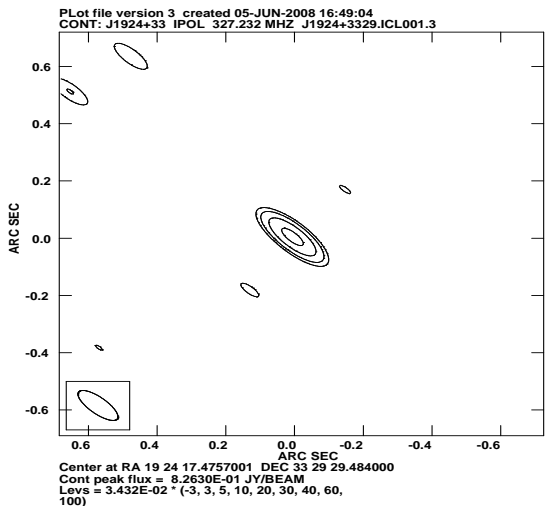
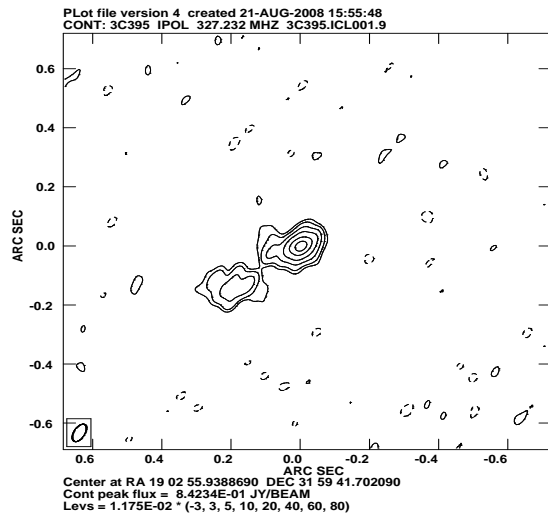
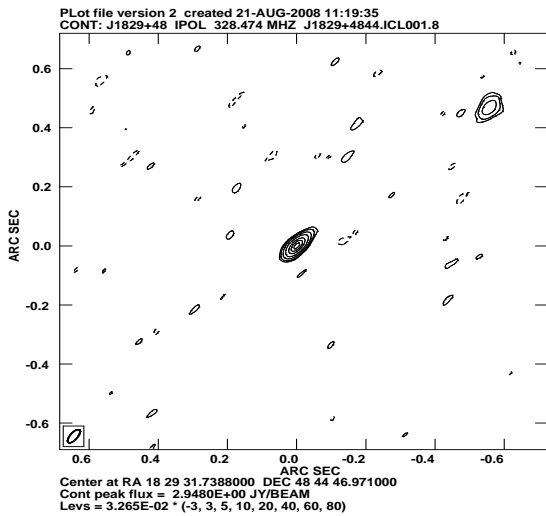
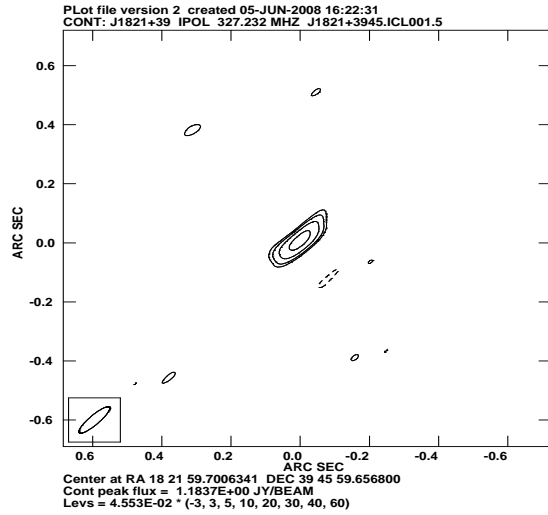
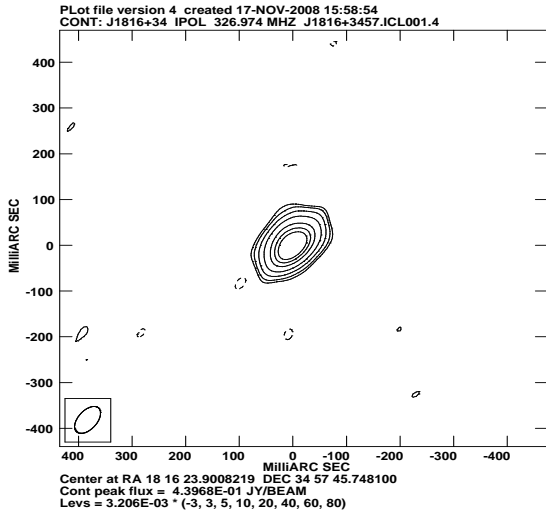


Fig. 5. Imaged sources at 327 MHz. The sources here in order are: J2022+6136, J2038+5119 (3C418), J2202+4216 (BL Lac), J2253+1608 (3C454.3), J2327+0940, J2330+11

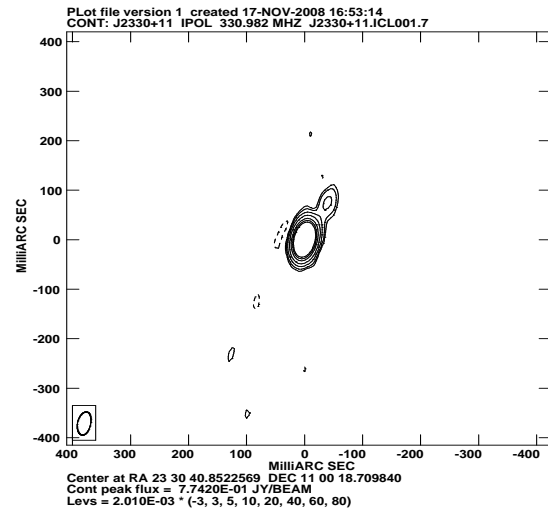
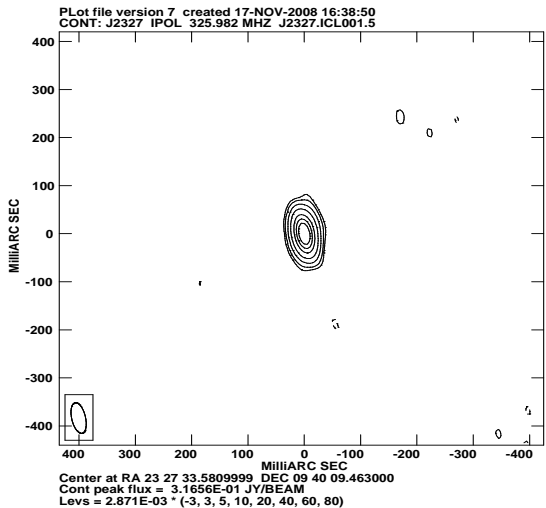
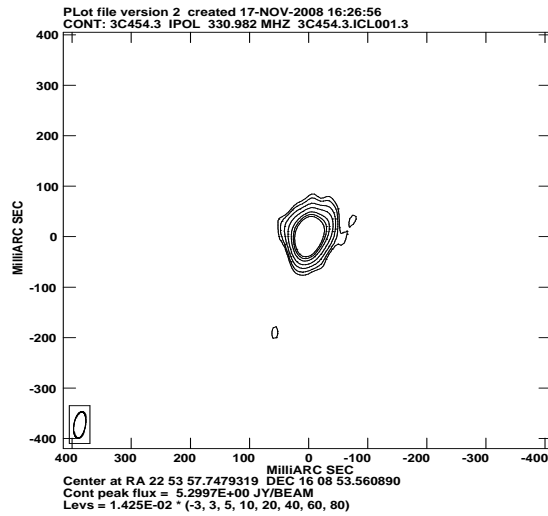
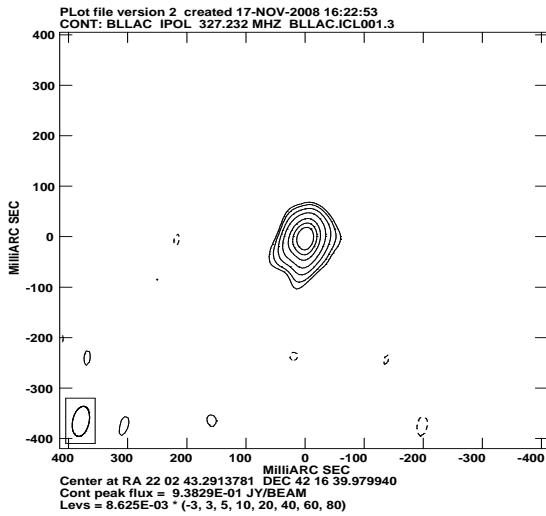
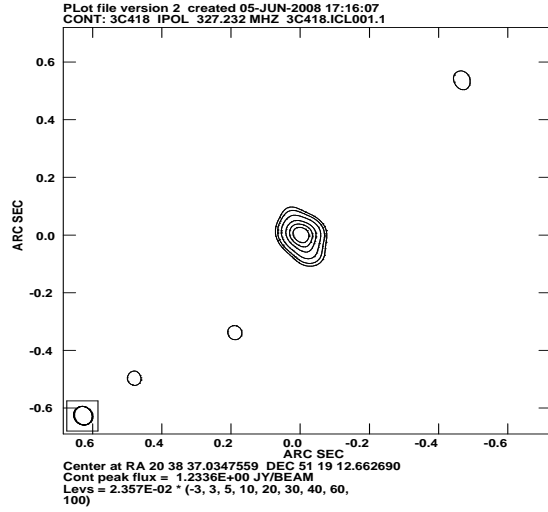
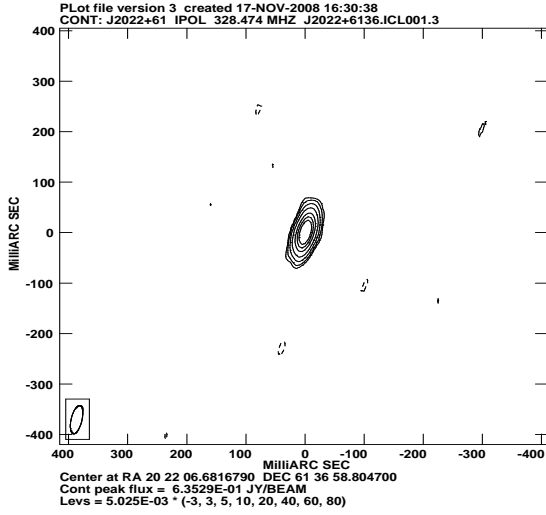


Fig. 6. Plots of flux density vs UV distance and UV plots for J0204+3649, J0319+4130 (3C84), J0405+3803

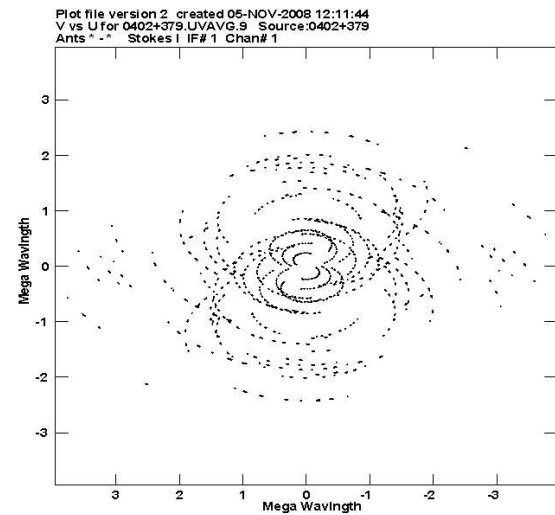
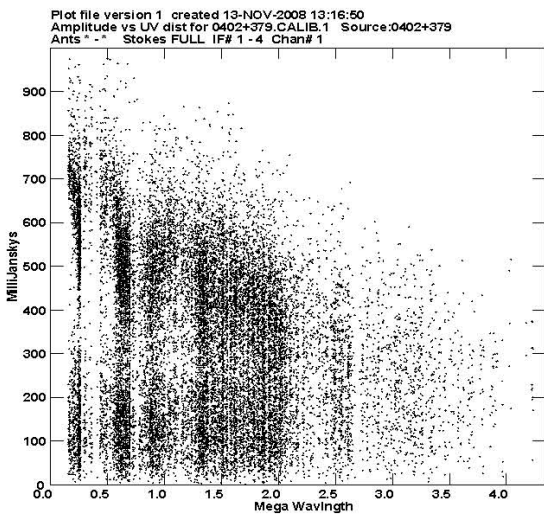
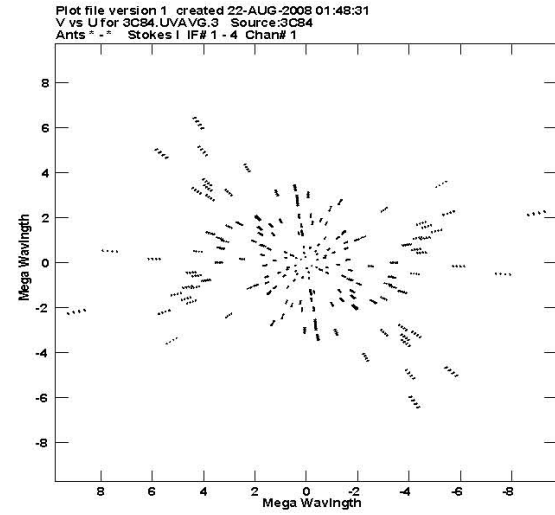
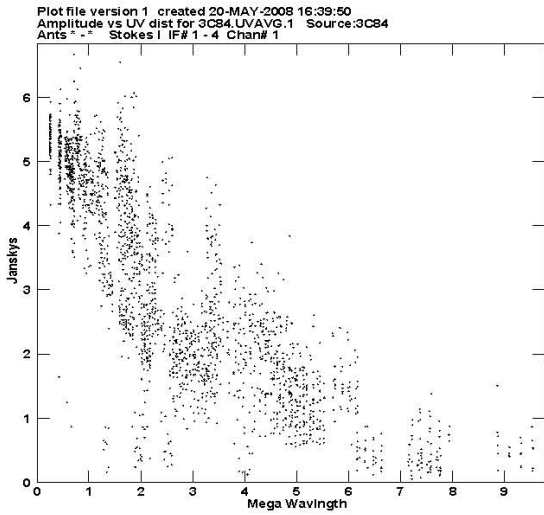
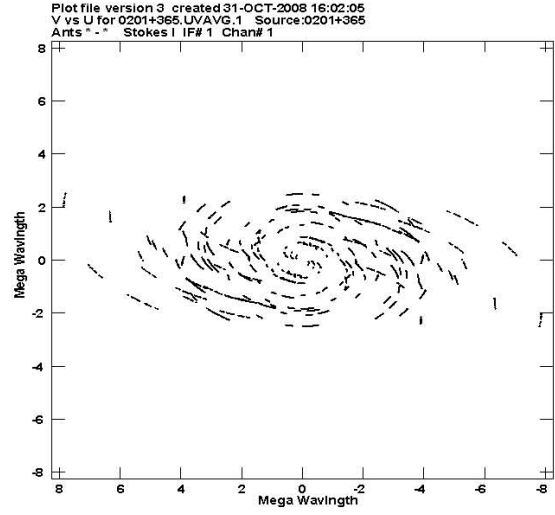
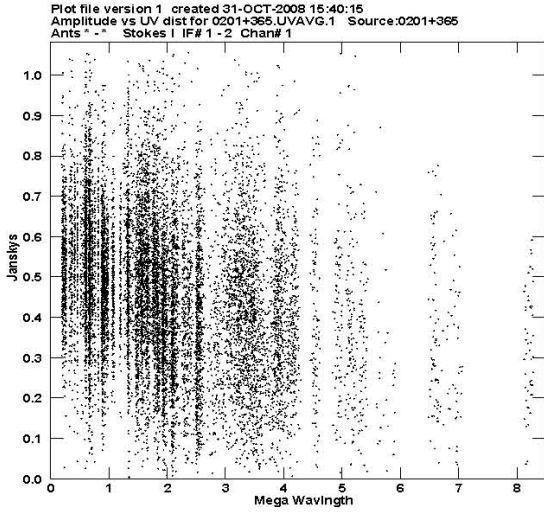


Fig. 7. Plots of flux density vs UV distance and UV plots for J0407-3303, J0418+3801 (3C111), J0423-0120

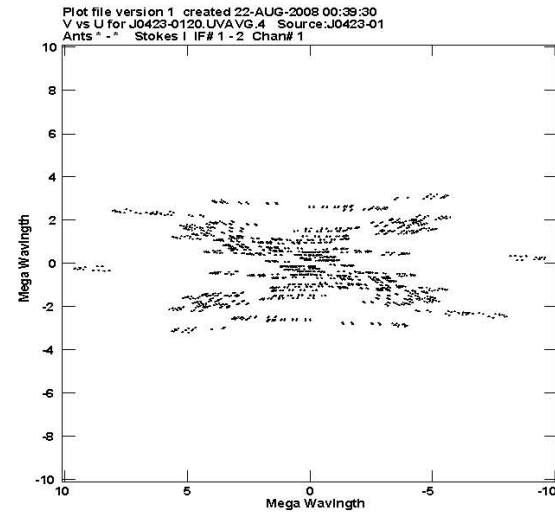
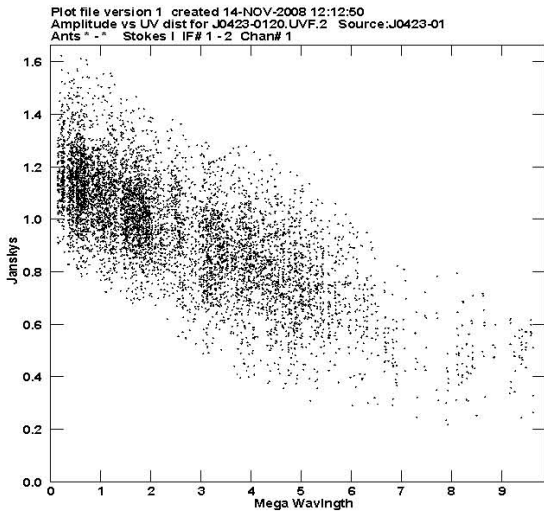
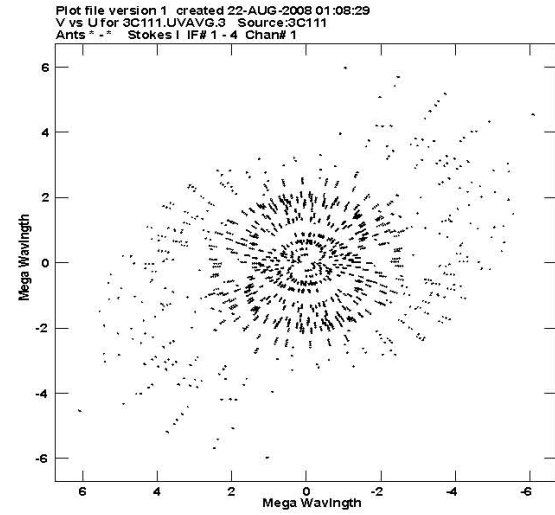
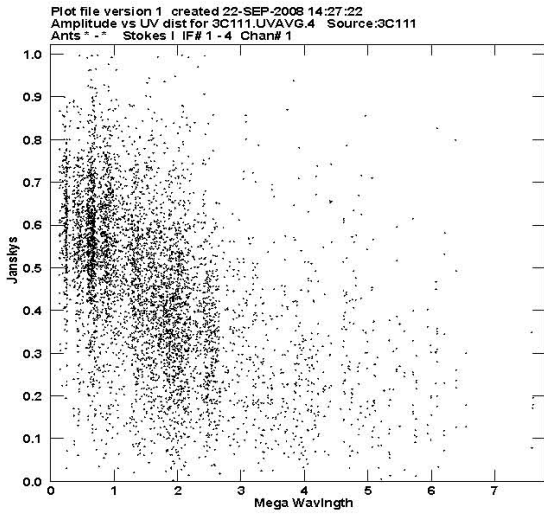
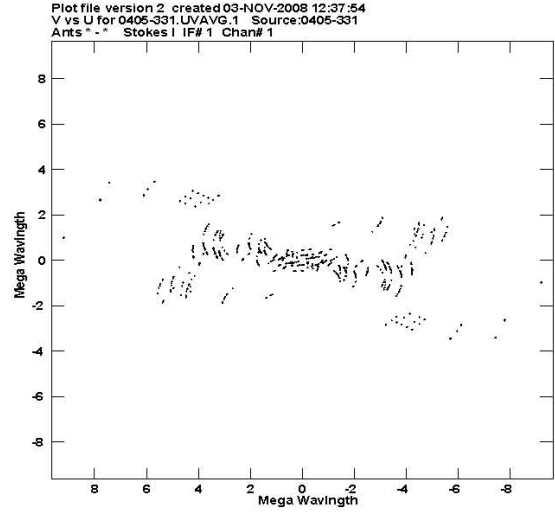
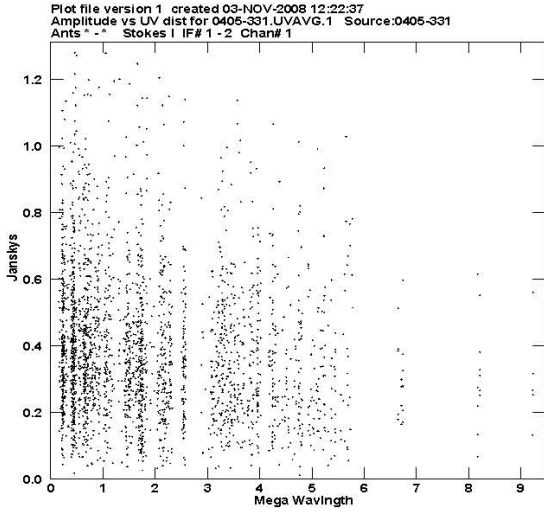


Fig. 8. Plots of flux density vs UV distance and UV plots for J0433+0521 (3C120), J0542+4951 (3C147), J0539-2839

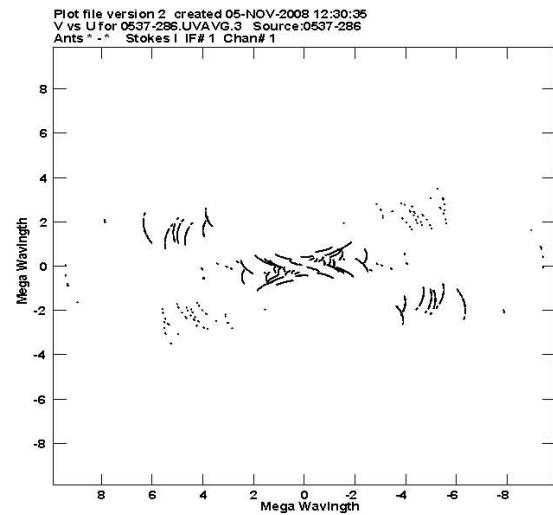
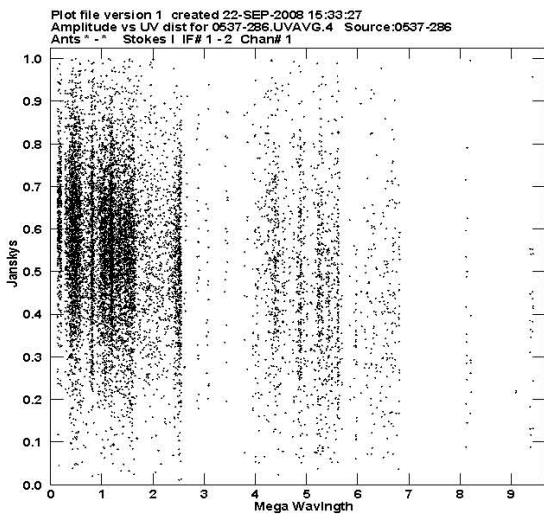
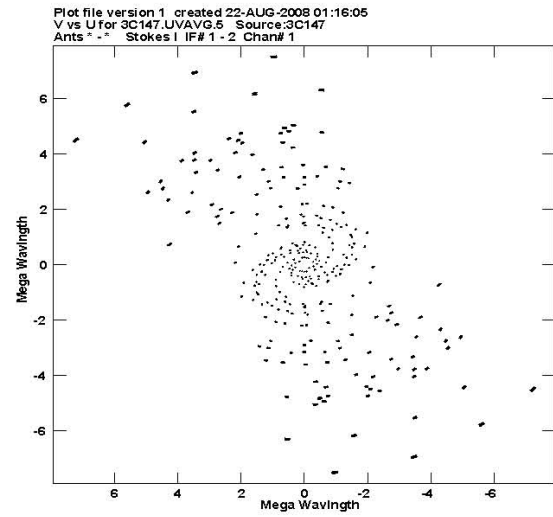
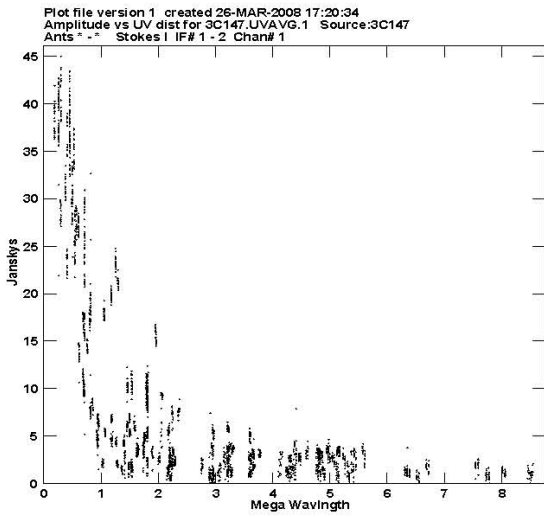
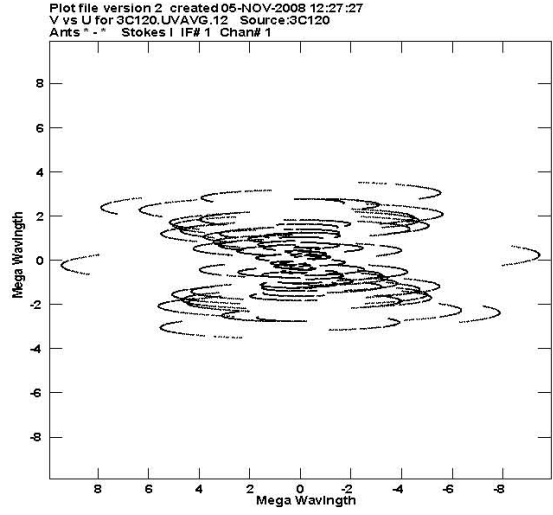
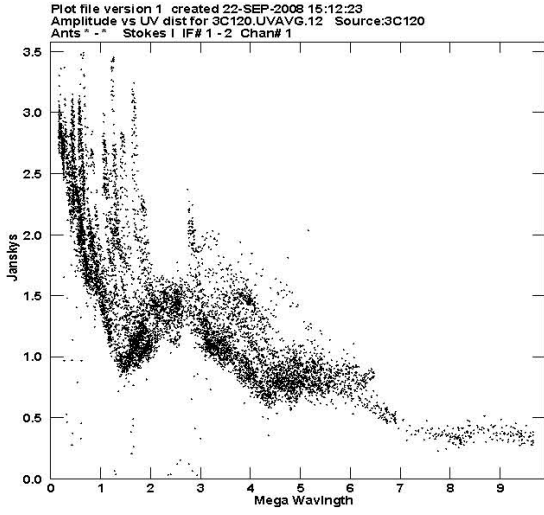


Fig. 9. Plots of flux density vs UV distance and UV plots for J1150-0024, J1230+1223 (3C274), J1229+0203 (3C273)

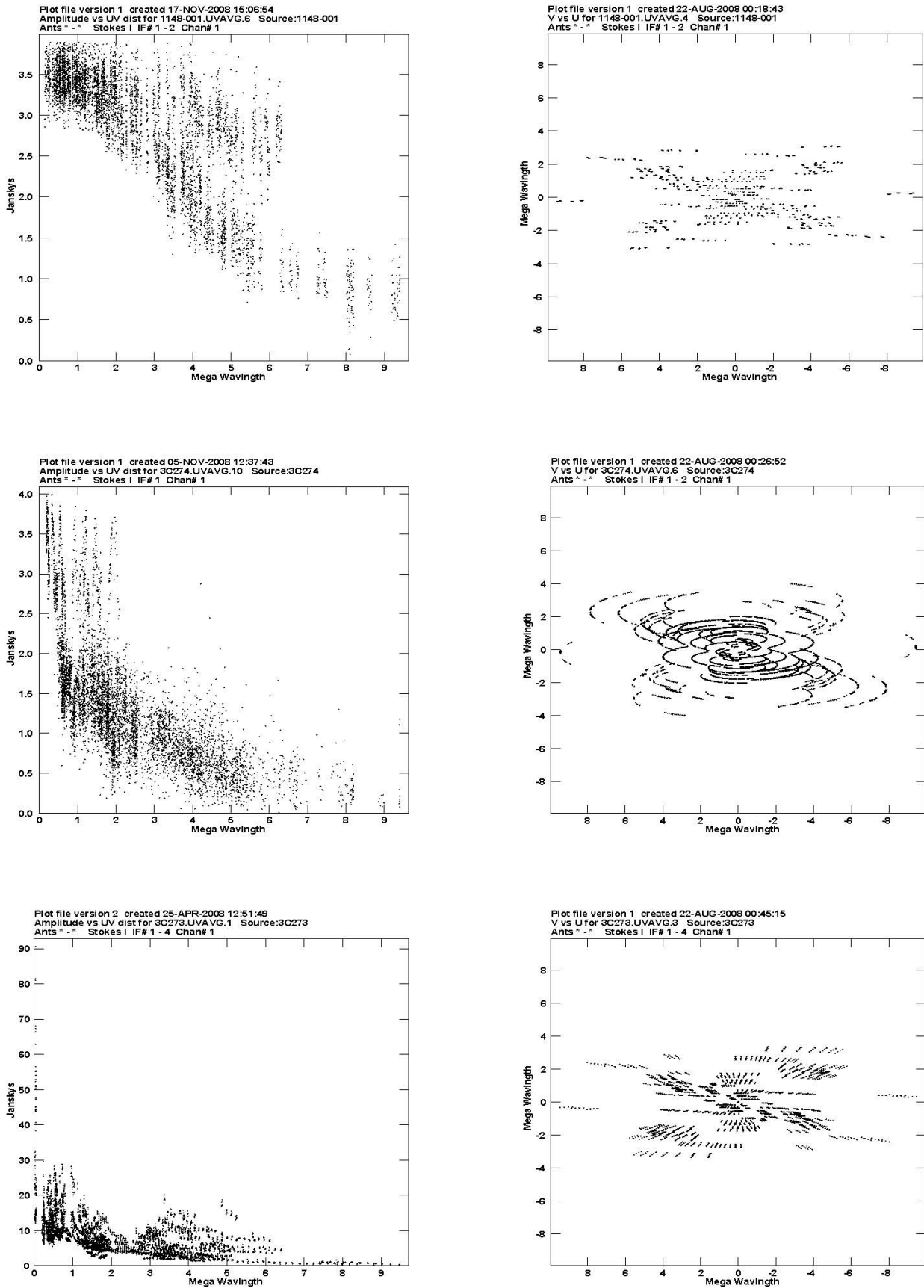


Fig. 10. Plots of flux density vs UV distance and UV plots for J1243+1622 (3C275.1), J1331+3030 (3C286), J1333+1649

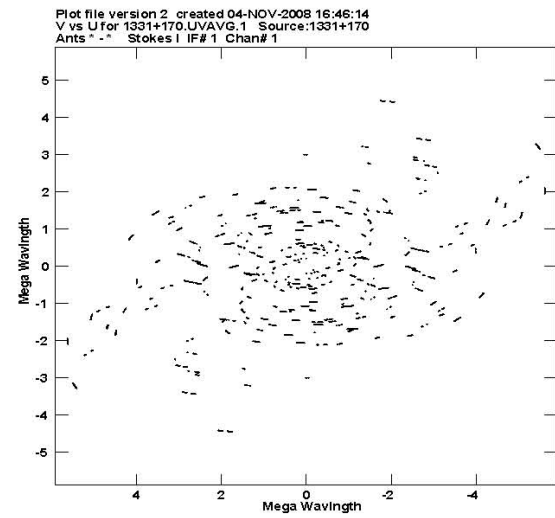
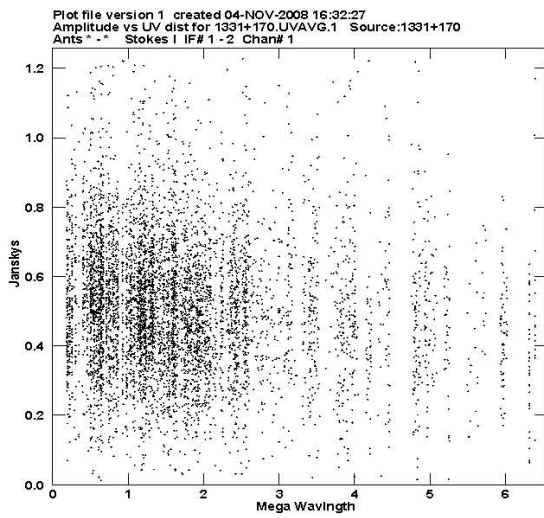
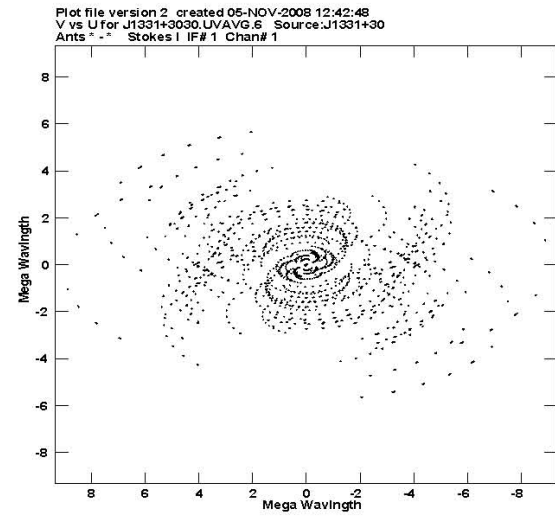
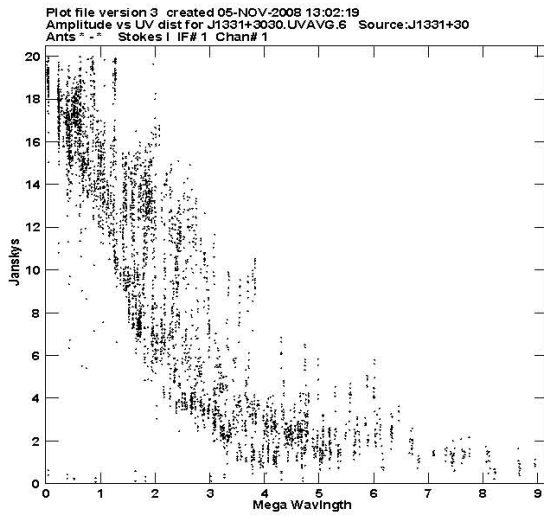
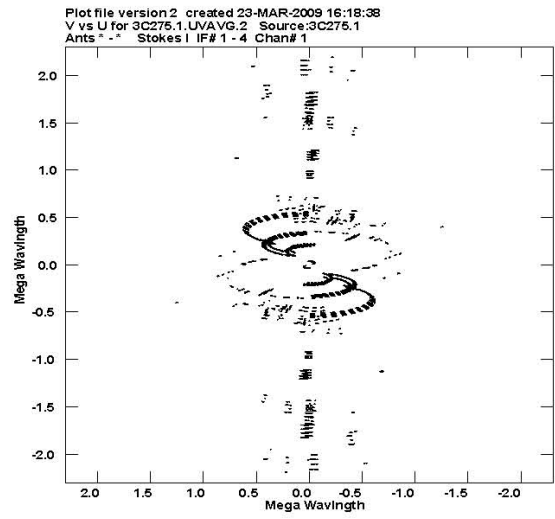
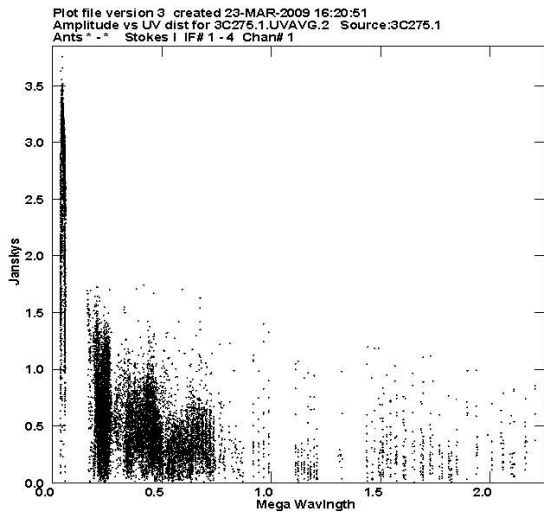


Fig. 11. Plots of flux density vs UV distance and UV plots for J1512-0905, J1642+3948 (3C345), J1746+6226

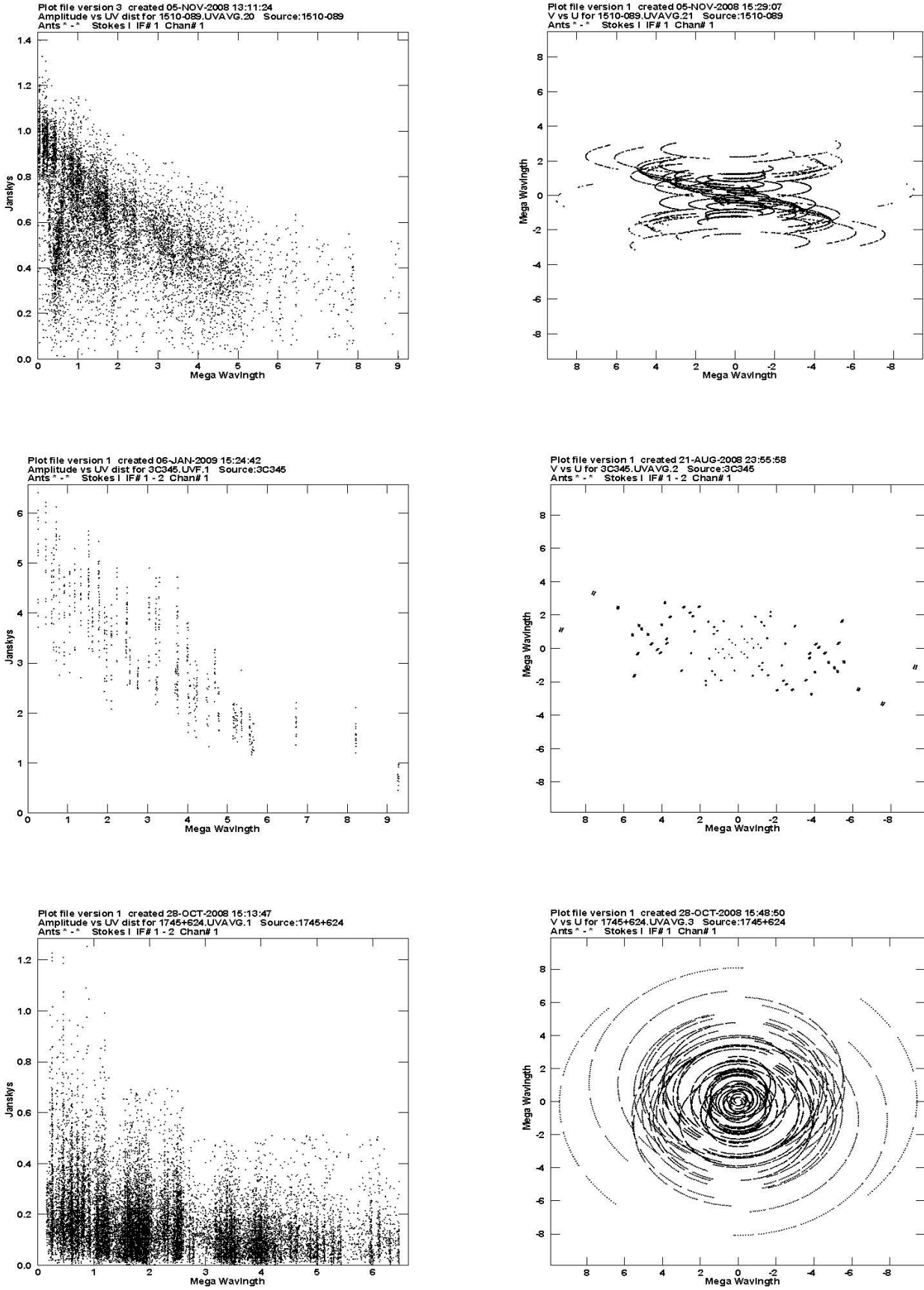


Fig. 12. Plots of flux density vs UV distance and UV plots for J1816+3457, J1821+3945, J1829+4844

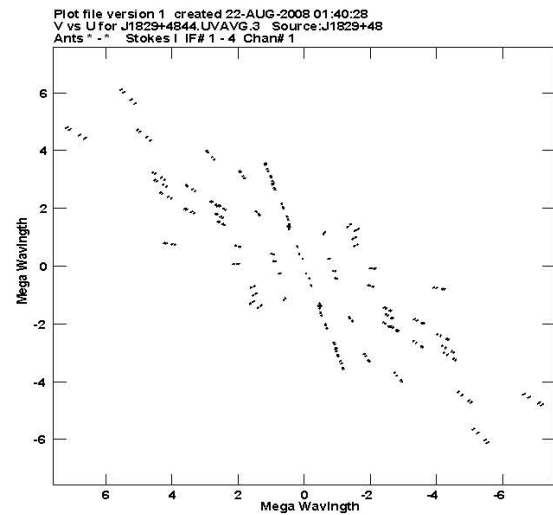
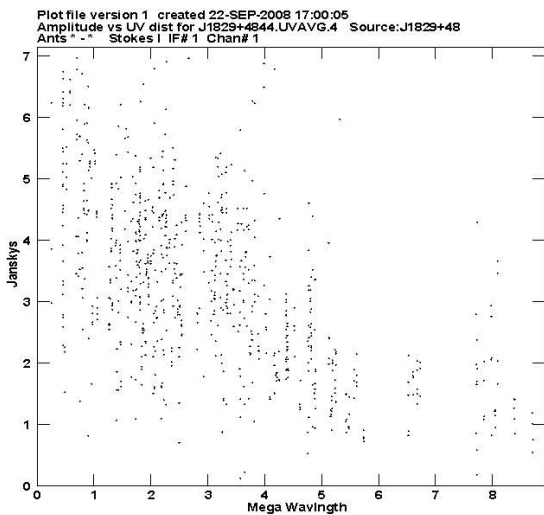
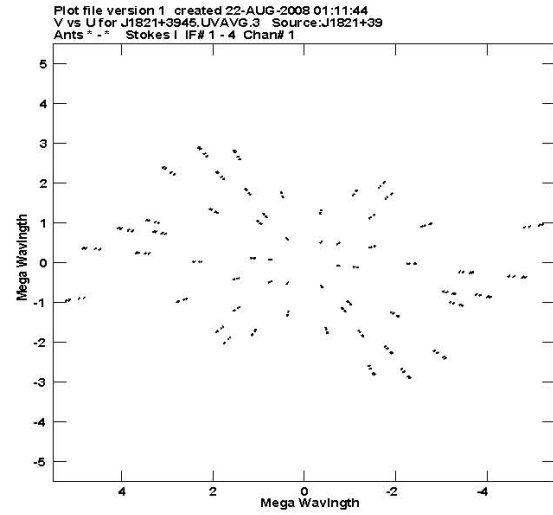
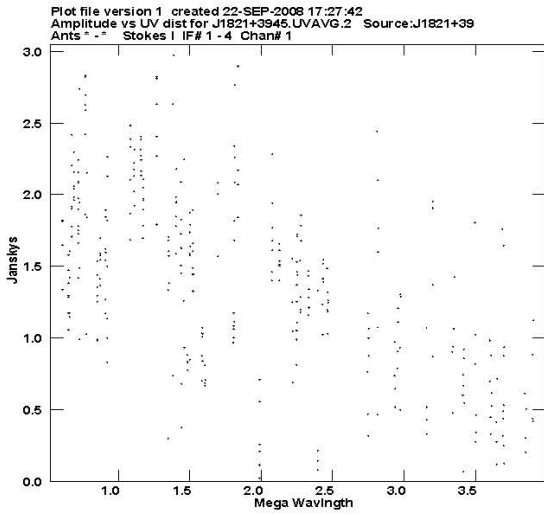
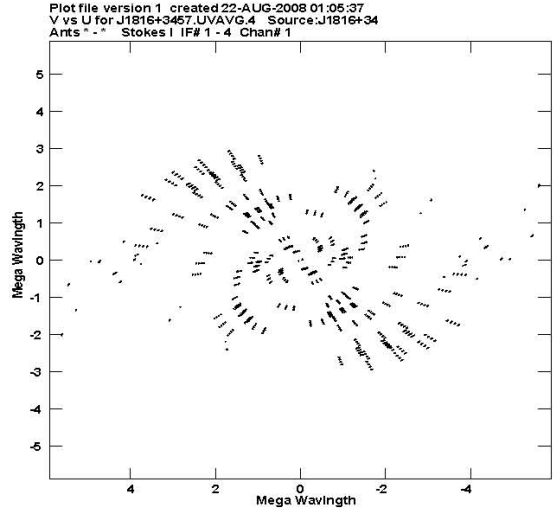
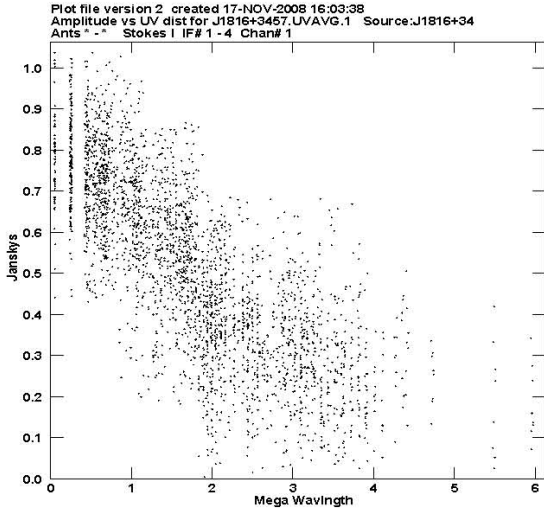


Fig. 13. Plots of flux density vs UV distance and UV plots for J1902+3159 (3C395), J1924+3329, J2005+7752

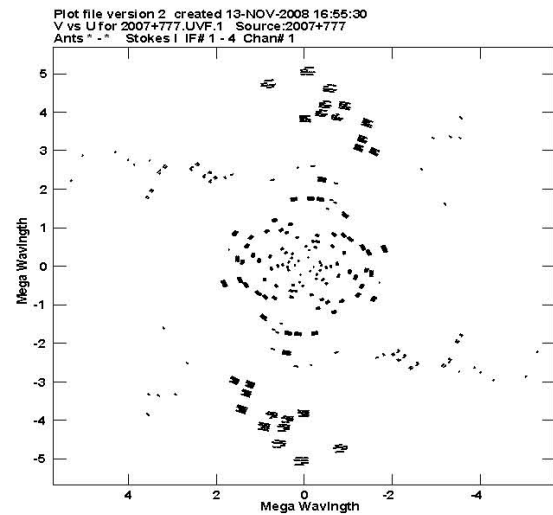
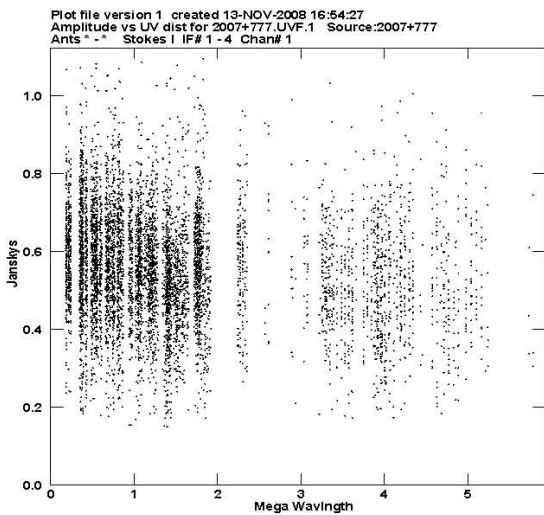
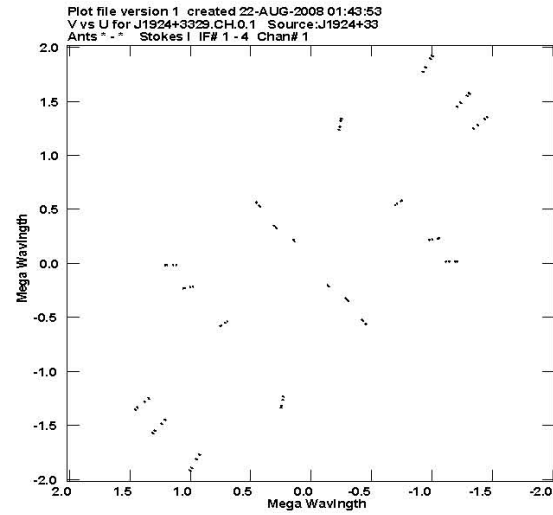
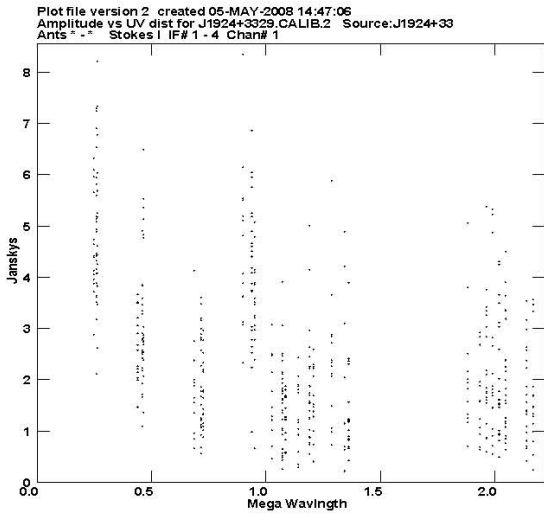
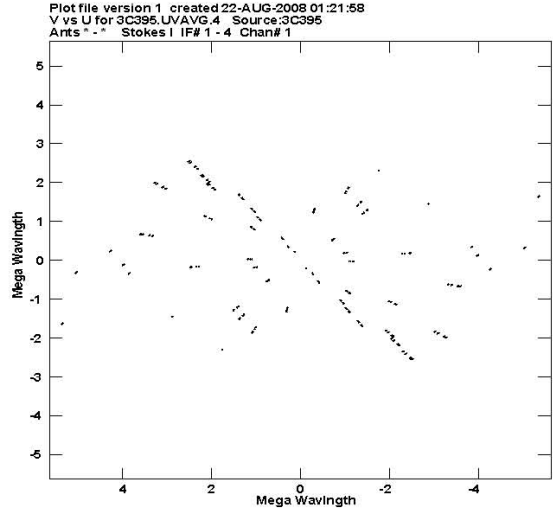
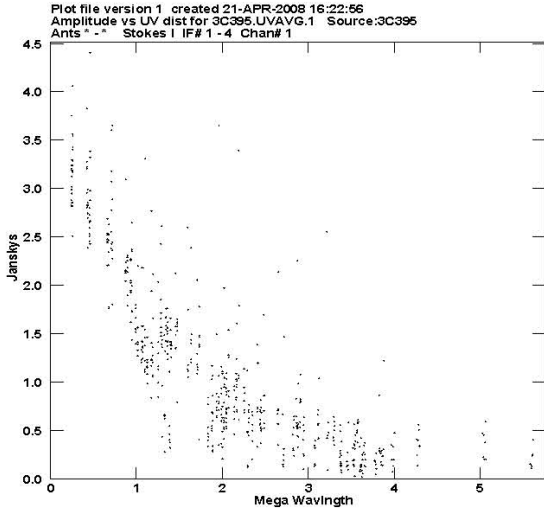


Fig. 14. Plots of flux density vs UV distance and UV plots for J2022+6136, J2038+5119 (3C418), J2202+4216 (BL Lac)

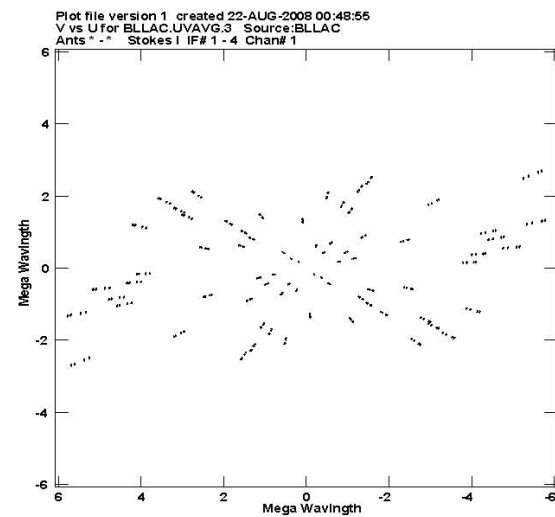
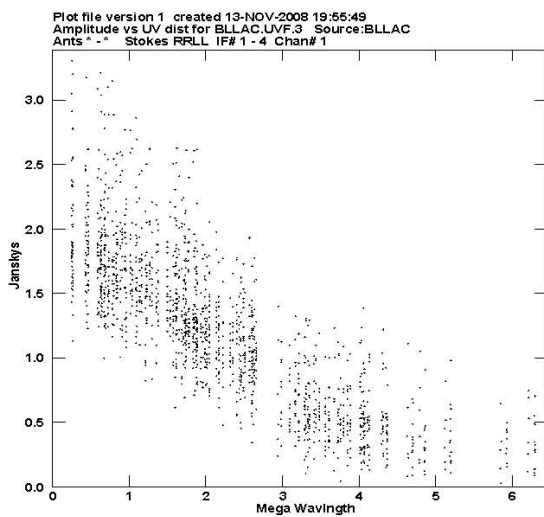
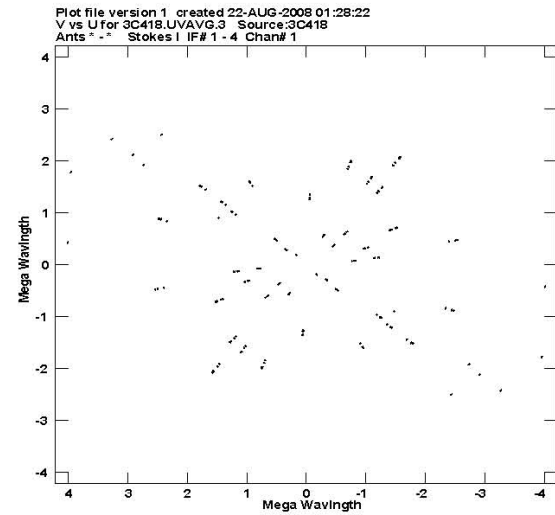
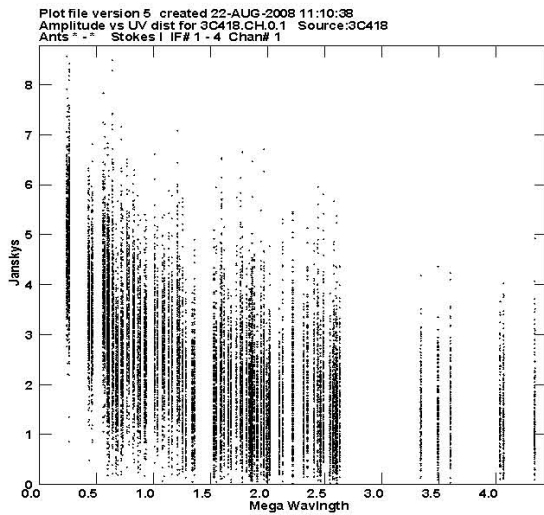
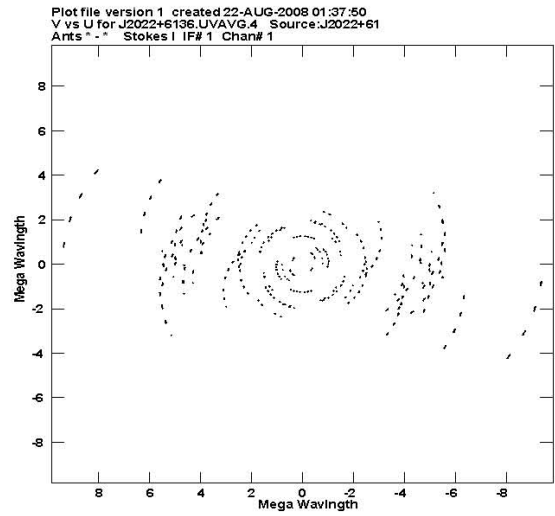
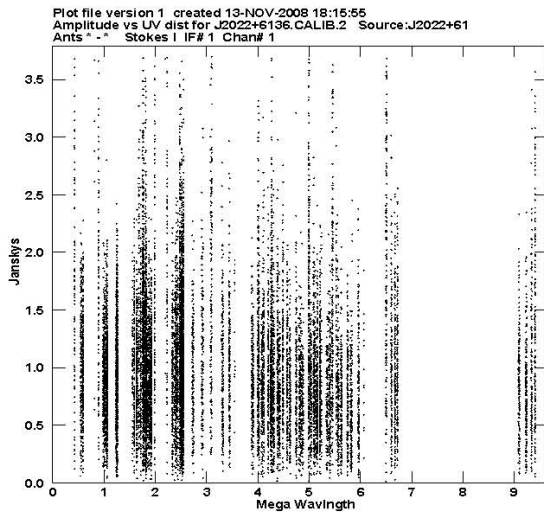


Fig. 15. Plots of flux density vs UV distance and UV plots for J2253+1608 (3C454.3), J2327+0940, J2330+11

